

# Northumbria Research Link

Citation: Wu, Dandan, Jia, Runping, Wen, Ming, Zhong, Shuai, Wu, Qingsheng, Fu, Richard and Yu, Shuhong (2020) Ultrastable PtCo/Co<sub>3</sub>O<sub>4</sub>-SiO<sub>2</sub> Nanocomposite with Active Lattice Oxygen for Superior Catalytic Activity toward CO Oxidation. *Inorganic Chemistry*, 59 (2). pp. 1218-1226. ISSN 0020-1669

Published by: American Chemical Society

URL: <https://doi.org/10.1021/acs.inorgchem.9b02937>  
<<https://doi.org/10.1021/acs.inorgchem.9b02937>>

This version was downloaded from Northumbria Research Link:  
<http://nrl.northumbria.ac.uk/id/eprint/41913/>

Northumbria University has developed Northumbria Research Link (NRL) to enable users to access the University's research output. Copyright © and moral rights for items on NRL are retained by the individual author(s) and/or other copyright owners. Single copies of full items can be reproduced, displayed or performed, and given to third parties in any format or medium for personal research or study, educational, or not-for-profit purposes without prior permission or charge, provided the authors, title and full bibliographic details are given, as well as a hyperlink and/or URL to the original metadata page. The content must not be changed in any way. Full items must not be sold commercially in any format or medium without formal permission of the copyright holder. The full policy is available online: <http://nrl.northumbria.ac.uk/policies.html>

This document may differ from the final, published version of the research and has been made available online in accordance with publisher policies. To read and/or cite from the published version of the research, please visit the publisher's website (a subscription may be required.)



**Northumbria  
University**  
NEWCASTLE



**UniversityLibrary**

**Submit to: Inorganic Chemistry**

**Ultra-stable PtCo/Co<sub>3</sub>O<sub>4</sub>-SiO<sub>2</sub> Nanocomposite with Active Lattice Oxygen for Superior Catalytic Activity towards CO Oxidation**

*Dandan Wu,<sup>†a,b</sup> Runping Jia,<sup>†b</sup> Ming Wen,<sup>\*a</sup> Shuai Zhong,<sup>a</sup> Qingsheng Wu,<sup>a</sup> Yongqing Fu<sup>c</sup> and Shuhong Yu<sup>d</sup>*

<sup>a</sup>School of Chemical Science and Engineering, Shanghai Key Laboratory of Chemical Assessment and Sustainability, Tongji University, 1239 Siping Road, Shanghai 200092, R. P. China.

<sup>b</sup>School of Materials Science and Engineering, Shanghai Institute of Technology, 100 Haiquan Road, Shanghai 201418, R. P. China.

<sup>c</sup>Faculty of Engineering and Environment, Northumbria University, Newcastle upon Tyne, NE1 8ST, UK.

<sup>d</sup>Department of Chemistry, University of Science and Technology of China, Hefei National Research Center for Physical Sciences at Microscale, 96 JinZhai Road, Hefei 230022, R. P. China.

**KEYWORDS**

PtCo/Co<sub>3</sub>O<sub>4</sub>-SiO<sub>2</sub>, flower-like structure, CO oxidation, active lattice oxygen, long-term durability

**ABSTRACT**

Nanostructural catalyst with long-term durability under harsh conditions is very important for outstanding catalytic performance. Herein, a new ultra-stable PtCo/Co<sub>3</sub>O<sub>4</sub>-SiO<sub>2</sub> nanocatalyst was explored to improve the catalytic performance of carbon monoxide (CO) oxidation in virtue of the active surface lattice oxygen derived from strong metal-support interactions. Such structure can overcome the issues of the Co<sub>3</sub>O<sub>4</sub>-SiO<sub>2</sub> inactivation by water vapor and the Pt inferior activity at low temperature. Further, Co<sub>3</sub>O<sub>4</sub>-SiO<sub>2</sub> nanosheets endow superior structure stability under a high temperature up to 800 °C, which gives the long-term catalytic cyclability of PtCo/Co<sub>3</sub>O<sub>4</sub>-SiO<sub>2</sub>

nanocomposites for CO oxidation. Moreover, the large specific surface areas (294 m<sup>2</sup>/g) of the nanosheet structure can expose abundant active surface lattice oxygen, which significantly enhanced the catalytic activity of CO oxidation at 50 °C over 30 days, and without apparent aggregation of PtCo nanoparticles after 20 cycles from 50 °C to 400 °C. It can be expected to be a promising candidate for ultra-stable efficient catalyst.

## 1. INTRODUCTION

Many industrial catalytic processes, including carbon monoxide (CO) oxidation, CH<sub>4</sub> combustion, catalytic hydrogenation reaction, etc., are generally carried out over 300 °C, therefore, designing high-temperature-resistant catalysts with good performance become critically demanded.<sup>1-5</sup> Till now, nanocatalysts containing Pt have still received extensive attention for these applications.<sup>6-9</sup> However, Pt nanoparticles (NPs) are easily aggregated for minimizing their surface energy at a high temperature, which could result in serious activity dropping of catalysts. To solve this problem, some methods have been proposed.<sup>10,11</sup> For example, Pt NPs have been dispersed onto the support with large surface areas (e.g., CeO<sub>2</sub> or Al<sub>2</sub>O<sub>3</sub>), and thus can realize enhanced utilization of active-atoms thereby improving the catalytic activity. But the catalytic activity remains to be improved at temperatures <100 °C.<sup>12-14</sup> So it is yet an arduous challenge to construct Pt included nanocatalysts with a long cyclability within a much wider temperature range.

Owing to the special structure features, various two-dimensional (2D) nanomaterials have been investigated globally in recent years.<sup>15,16</sup> Hereinto, non-noble-metals nanosheets with an atomic-layer thickness, especially those with defective ones, have been proposed as a promising candidate to improve catalytic performance due to their abundant catalytic active sites.<sup>17-21</sup> It has been demonstrated that ultrathin CeO<sub>2</sub> nanosheets with surface pits

can exhibit an outstanding catalytic activity for CO oxidation.<sup>22</sup> However, it is difficult to maintain 2D nanostructure and activity at a high temperature because of high surface energy, which significantly restrict their practical catalysis applications. In order to stabilize the active components, silica ( $\text{SiO}_2$ ) has been widely applied as a support or a shell in the heterogeneous catalysts, but this is still not good enough to restrain the aggregation of active components or to contact well with catalytic substrates.<sup>23-25</sup> To address the above issues, one way is to fabricate the 2D nanocomposite with the catalytic active components separated by  $\text{SiO}_2$  nanosheets, which can not only increase the stability of active species, but also enlarge surface areas for the effective utilization of active atoms.

In this work, a unique heterostructure of  $\text{PtCo}/\text{Co}_3\text{O}_4\text{-SiO}_2$  has been designed and successfully constructed through a galvanic replacement coprecipitation process followed by  $\text{H}_2$  reduction, in which insitu alloying of PtCo anchored on  $\text{Co}_3\text{O}_4\text{-SiO}_2$  nanosheets results in abundant active lattice oxygens. Such structure is expected to improve the catalytic activity of Pt at low temperature, meanwhile to overcome the catalysis limitation of  $\text{Co}_3\text{O}_4$  under water vapour for CO oxidation. Thus, the obtained  $\text{PtCo}/\text{Co}_3\text{O}_4\text{-SiO}_2$  catalysts can give rise to the following advantages for CO oxidation: i) Such nanoflower-like structure assembled by nanosheets leads to a mass of channels and large surface areas, which are beneficial for gas flow thereby immensely improving the catalyzation of CO oxidation; ii) The excellent thermal-stability of  $\text{Co}_3\text{O}_4\text{-SiO}_2$  nanosheets can ensure the steady structure even at a high-temperature over 800 °C for long cycling catalytic activity; iii) The strong metal-support interactions (SMSI) between PtCo and  $\text{Co}_3\text{O}_4\text{-SiO}_2$  can generate plentiful active lattices oxygens, which enable to significantly enhance catalytic performance at low temperature under water vapour. Therefore, the  $\text{PtCo}/\text{Co}_3\text{O}_4\text{-SiO}_2$

structures exhibit an excellent stability at a high temperature, meanwhile, overcome the both issues of the  $\text{Co}_3\text{O}_4\text{-SiO}_2$  inactivation by water vapor and the Pt inferior activity at low temperature. This work explores a new route in the development of ultra-stable hetero-nanocatalysts with 2D self-assembled structure for efficiently catalyzing CO oxidation at a wide temperature range in virtue of the active centers derived from SMSI.

## **2. EXPERIMENT SECTION**

### **2.1. Chemicals**

Copper chloride dihydrate ( $\text{CuCl}_2\cdot 2\text{H}_2\text{O}$ , 99%), ethanol ( $\text{C}_2\text{H}_5\text{OH}$ , 99%), acetone ( $\text{C}_3\text{H}_6\text{O}$ , 99.5%) and chloroplatinic acid hexahydrate ( $\text{H}_2\text{PtCl}_6\cdot 6\text{H}_2\text{O}$  with Pt content  $\geq 37\%$ ) were purchased from Sinopharm Chemical Reagent Co., Ltd., China. Cobalt chloride hexahydrate ( $\text{CoCl}_2\cdot 6\text{H}_2\text{O}$ , 99.7%), sodium borohydride ( $\text{NaBH}_4$ , 98%), urea ( $\text{CH}_4\text{N}_2\text{O}$ , 99%) and hydrofluoric acid ( $\text{HF}$ ,  $\geq 40\%$ ) were purchased from Aladdin Reagents, Shanghai, China. All reagents were used without further purification. The silicon wafers were purchased from Zhejiang Lijing Silicon Material Co., Ltd. China., and cleaned with acetone, ethanol, and then the deionized water for three times before the usage.

### **2.2. Synthesis of $\text{Co}_3\text{O}_4\text{-SiO}_2$ nanoflower-spheres**

The  $\text{Co}_3\text{O}_4\text{-SiO}_2$  nanoflower-spheres catalyst was synthesized by a modified hydrothermal method. The typical synthesis process is described as follows:  $\text{CoCl}_2\cdot 6\text{H}_2\text{O}$  aqueous solution (15 mL, 5 mM) and  $\text{CuCl}_2\cdot 2\text{H}_2\text{O}$  aqueous solution (5 mL, 5 mM) were mixed in a Teflon-lined stainless steel autoclave. Then, a piece of  $1\text{cm}\times 1\text{cm}$  silicon wafer and 200 mg of urea were added. After magnetic stirring for 10 min, the reaction system was sealed and heated at  $140\text{ }^\circ\text{C}$  in an oven for 8 hrs with a heating rate of  $1\text{ }^\circ\text{C}\cdot\text{min}^{-1}$ . When the oven was cooled down to room temperature, the obtained products in the autoclave except for silicon wafer was collected by centrifugation,

and then alternately washed by ethanol and deionized water for three times and dried in a vacuum oven at 60 °C for 24 hrs. The  $\text{Co}_3\text{O}_4\text{-SiO}_2$  catalyst was obtained by calcinating the dried powder in air at 600 °C for 5 hrs. In addition, 3D radial needle-like  $\text{Co}_3\text{O}_4$  would be obtained, when only  $\text{CoCl}_2\cdot 6\text{H}_2\text{O}$  aqueous solution (15 mL, 5 mM) and urea (200 mg) were added to the Teflon-lined stainless steel autoclave.

### **2.3. Synthesis of PtCo/ $\text{Co}_3\text{O}_4\text{-SiO}_2$ nanocomposite**

In a typical preparation process, 50 mg of as-obtained  $\text{Co}_3\text{O}_4\text{-SiO}_2$  nanocomposite was added to HF solution (10 mL, 0.04%) and stirred for 20 min; then the suspension was washed with deionized water. After that,  $\text{H}_2\text{PtCl}_6$  solution (5 mL, 5 mM) was added to the washed suspension and subsequently ultrasonically dispersed for 2 hrs. The obtained solution was then placed in the freezer to ice-cold and rapidly injected a freshly prepared and ice-cold  $\text{NaBH}_4$  aqueous solution (10 mL, 10 mM) under vigorous stirring. The resulting mixture was then left at room temperature for 5 hrs and the final precipitates of Pt/ $\text{Co}_3\text{O}_4\text{-SiO}_2$  nanocomposites were collected by centrifugation and washed thoroughly. By further reducing Pt/ $\text{Co}_3\text{O}_4\text{-SiO}_2$  nanocomposite in 5%  $\text{H}_2$  at 400 °C for 1hr with a heating rate of 10 °C·min<sup>-1</sup>, PtCo/ $\text{Co}_3\text{O}_4\text{-SiO}_2$  nanocomposite catalyst can be obtained.

For comparison, the flower-like nanostructure of PtCo<sub>sync</sub>/ $\text{Co}_3\text{O}_4\text{-SiO}_2$  were also prepared by co-reduction alloy method, in which PtCo NPs were directly loaded on  $\text{Co}_3\text{O}_4\text{-SiO}_2$  nanosheet. The specific synthetic steps were as follows: 50 mg  $\text{Co}_3\text{O}_4\text{-SiO}_2$  nanocomposite was added to HF solution (10 mL, 0.04%) and stirred for 20 min; then the suspension was washed with deionized water. After that,  $\text{H}_2\text{PtCl}_6\cdot 6\text{H}_2\text{O}$  aqueous solution (5 mL, 5 mM) and  $\text{CoCl}_2\cdot 6\text{H}_2\text{O}$  aqueous solution (2 mL, 5 mM) were added to the washed suspension, and ultrasonically agitated for 2 hrs. The obtained solution was then placed in the freezer to ice-cold, and a freshly prepared, ice-cold

NaBH<sub>4</sub> aqueous solution (10 mL, 10 mM) was then rapidly injected under a vigorous stirring. The solutions was precipitated at room temperature for 5 hrs, and the precipitates were centrifuged, washed with deionized water and absolute ethanol repeatedly, and then dried in a vacuum oven at 60 °C for 24 hrs to obtain PtCo<sub>sync</sub>/Co<sub>3</sub>O<sub>4</sub>-SiO<sub>2</sub> nanocomposite catalyst.

#### **2.4. Characterization**

Field-emission scanning electron microscope (SEM, JEOL, S-4800) was used to investigate the morphology of the samples, and elemental compositions were analyzed by using an energy dispersive X-ray spectroscope (EDS), which was conducted at 20 keV on a TN5400 EDS instrument (Oxford). Microstructures of the materials were studied by using a high-resolution transmission electron microscope (HRTEM, JEOL JEM-2100EX, Japan). Powder X-ray diffraction (XRD) patterns were obtained by using a Bruker D8 (German) diffractometer with a Cu K $\alpha$  radiation source ( $\lambda$ = 0.1541 nm) and a scanning angle ( $2\theta$ ) of 10°-90°, operated at 40 kV and 40 mA. The chemical states of elements were analyzed by using an X-ray photoelectron spectroscope (XPS, RBD-upgraded PHI-5000C ESCA system, Perkin Elmer) with Mg K $\alpha$  radiation ( $h\nu$ =1486.6 eV). Before analyzing the XPS peaks, the binding energies of all the elements were calibrated using the containment carbon (C 1s=284.6 eV) as the reference. The deconvolution of the XPS spectra was performed after subtracting the background of each peak using the Shirley. The Brunauer–Emmett–Teller (BET) surface areas were measured using the Micromeritics TRISTAR 3020. H<sub>2</sub> temperature-programmed reduction (H<sub>2</sub>-TPR) was carried out on a Micromeritics AutoChem II 2920 automated catalyst characterization system. CO adsorption diffuse reflectance infrared Fourier-transform spectroscopy (CO DRIFTS) was performed on PerkinElmer Frontier FT-IR.

#### **2.5. CO oxidation measurements**

The activities of catalysts for CO oxidation were evaluated in a continuous flow fixed-bed quartz reactor under an atmospheric pressure. 50 mg catalysts were pressed, crushed, and sieved to the 40-60 mesh size range and diluted with 200 mg of quartz sand. The operation temperature was controlled using a thermocouple and adjusted in the range of 30 °C to 400 °C. Temperatures used in the catalytic tests were measured using a second thermocouple placed in the catalyst bed. Before each measurement, the catalysts were pre-treated with N<sub>2</sub> gas (50 ml·min<sup>-1</sup>) at 300 °C for 1 hr, then a 2.0 vol.% CO/10 vol.% O<sub>2</sub>/N<sub>2</sub> mixture (50 ml·min<sup>-1</sup>) was introduced into the reactor, which corresponds to a gas hourly space velocity(GHSV) of 60,000 h<sup>-1</sup>. The reactants and products were analyzed using on-line A90 gas chromatography (Shanghai Yimeng Electronic Technology Co., Ltd.). The column was a stainless steel tube with a diameter of 3 mm and was filled with a carbon molecular sieve chromatography packing. The detector used was a thermal conductivity detector (TCD). And the details of the equipment are shown in scheme S1. The catalytic oxidation activity of the catalyst is represented by the conversion rate of CO<sub>2</sub> generated by CO. The CO light-off temperature is 50% of CO conversion and represented by T<sub>50</sub>; and the lowest complete conversion temperature of the CO is represented by T<sub>100</sub>. The conversion rate (C) was calculated according to the following formula:  $C = \frac{n(\text{CO}_{\text{in}}) - n(\text{CO}_{\text{out}})}{n(\text{CO}_{\text{in}})}$

For a typical light-off run, the temperature was ramped with a rate of 2 °C·min<sup>-1</sup> from 30 °C to 400 °C, and the data collection was performed after every 5 °C. Prior to data recording for each experiment, the temperature was stabilized for 5 min.

In a typical steady-state experiment, the system was adjusted to the measured temperature under N<sub>2</sub> flow at a heating rate of 10 °C·min<sup>-1</sup>, and then replaced by the reaction mixture gas. The data were recorded every 12 hrs.

In a standard cycle experiment, the temperature was increased from 50 °C to 400 °C with a step of 25 °C. Before the measurement, the temperature was controlled to stabilize for 5 min. Once a cycle was finished, the reactor was cooled down to room temperature before new cycle was started.

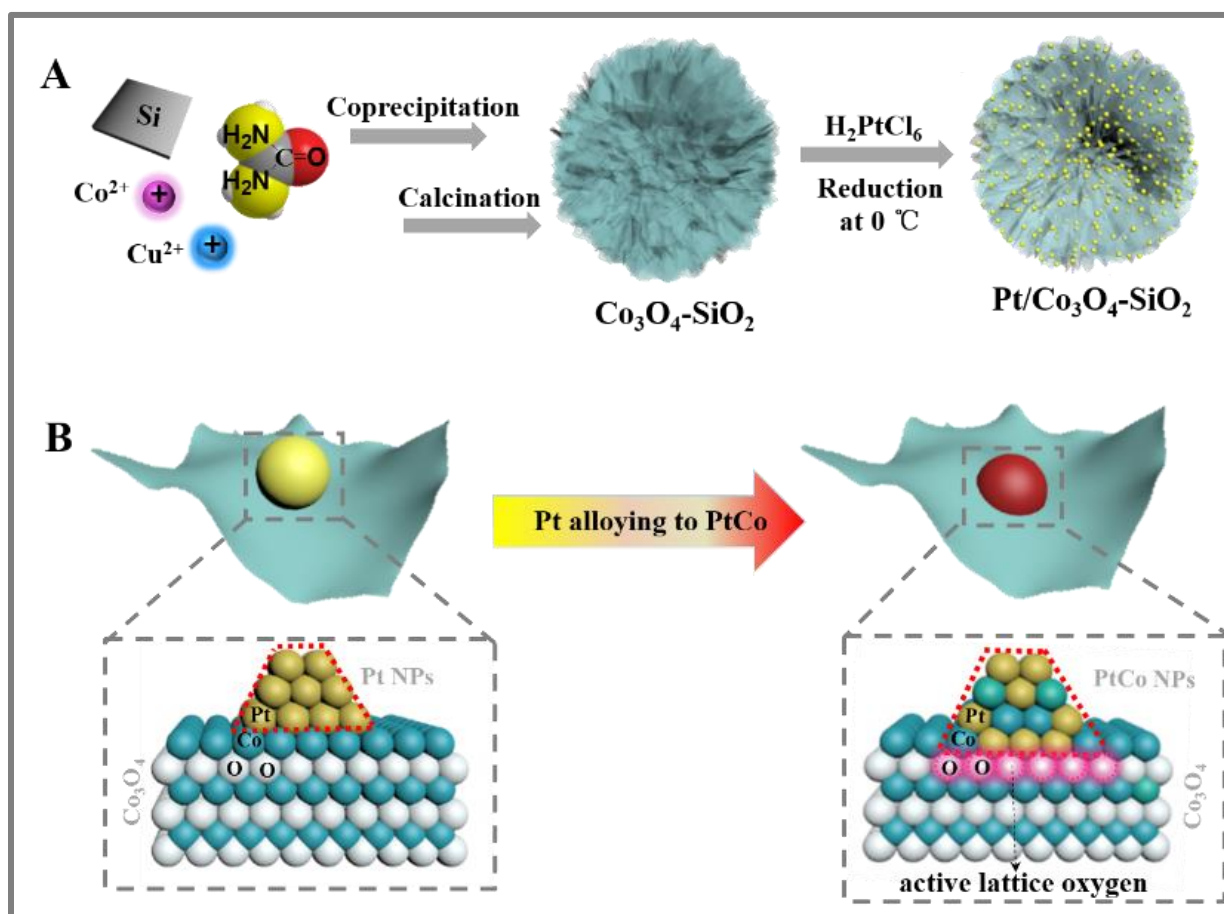
### 3. RESULTS AND DISCUSSION

#### 3.1. Mechanism of fabrication

The flower-like nanostructures of PtCo/Co<sub>3</sub>O<sub>4</sub>-SiO<sub>2</sub> have been successfully constructed, in which the structures were self-assembled by Co<sub>3</sub>O<sub>4</sub>-SiO<sub>2</sub> nanosheets with embedded PtCo nanoalloys (NAs) via the insitu reduction of H<sub>2</sub>, as shown in Scheme 1. Firstly, Co<sub>3</sub>(Si<sub>2</sub>O<sub>5</sub>)<sub>2</sub>(OH)<sub>2</sub> nanoflower-spheres, the precursor of the Co<sub>3</sub>O<sub>4</sub>-SiO<sub>2</sub> nanocomposites, were fabricated by galvanic replacement coprecipitation process in a hydrothermal system. The reaction is initiated by the hydrolysis of urea, the subsequent product of NH<sub>3</sub> hydrolyzes to produce OH<sup>-</sup> and react with Co<sup>2+</sup> & SiO<sub>3</sub><sup>2-</sup>. Then Co<sub>3</sub>(Si<sub>2</sub>O<sub>5</sub>)<sub>2</sub>(OH)<sub>2</sub> precursor were obtained, in which SiO<sub>3</sub><sup>2-</sup> was derived from the replacement of Cu<sup>2+</sup> with Si on the surface of silicon wafer, because  $\phi_{\text{Cu}^{2+}/\text{Cu}}$  (-0.222 V) is much higher than  $\phi_{\text{SiO}_3^{2-}/\text{Si}}$  (-1.697 V) in the alkaline solution. After the reaction, the surface of silicon wafer was then chemically deposited by a layer of copper, which can be confirmed by XRD analysis (Figure S1). As the surface of silicon wafer covered by a layer of Cu, Co<sub>3</sub>(Si<sub>2</sub>O<sub>5</sub>)<sub>2</sub>(OH)<sub>2</sub> complex was preferred to grow in the solution, rather than on the silicon wafer. In the hydrothermal reaction, the Cu<sup>2+</sup> ions can not only control the generation rate of SiO<sub>3</sub><sup>2-</sup>, but also react with NH<sub>3</sub> to form [Cu(NH<sub>3</sub>)<sub>4</sub>]<sup>2+</sup>, therefore restrict the hydrolysis of NH<sub>3</sub> and then further control the co-precipitation rate of Co<sup>2+</sup> and SiO<sub>3</sub><sup>2-</sup>, which finally lead to the formation of 2D Co<sub>3</sub>(Si<sub>2</sub>O<sub>5</sub>)<sub>2</sub>(OH)<sub>2</sub> nanosheets precursor. In order to optimize the synthesis method and demonstrate the synthesis mechanism, we have selected different specifications

of silicon wafers and different additions of  $\text{Cu}^{2+}$  to react. The SEM was used to observe the morphologies of obtained samples, as shown in Figure S2 and S3. After the calcination, the precursors can be transformed into  $\text{Co}_3\text{O}_4\text{-SiO}_2$  nanocomposites. Secondly, after treatment with HF,  $\text{PtCl}_6^{2-}$  was absorbed on  $\text{Co}_3\text{O}_4\text{-SiO}_2$  nanosheets then to be in-situ reduced and form  $\text{Pt}/\text{Co}_3\text{O}_4\text{-SiO}_2$  composites. Finally, the further  $\text{H}_2$  treatment gives rise to the heterostructured of  $\text{PtCo}/\text{Co}_3\text{O}_4\text{-SiO}_2$ , in which Pt induced the reduction of Co from the surrounding  $\text{Co}_3\text{O}_4$  to form PtCo NAs, and results in the generation of active lattice oxygens as shown in Scheme 1B.<sup>26,27</sup>

**Scheme 1. Schematic illustration of the fabrication process of  $\text{PtCo}/\text{Co}_3\text{O}_4\text{-SiO}_2$  heterostructure.**



### 3.2. Morphologies and Structures

Morphologies and structures of PtCo/Co<sub>3</sub>O<sub>4</sub>-SiO<sub>2</sub> nanocomposites and contrast samples (Pt/Co<sub>3</sub>O<sub>4</sub>-SiO<sub>2</sub> and Co<sub>3</sub>O<sub>4</sub>-SiO<sub>2</sub>) are characterized, shown in Figure 1. It can be clearly observed that Co<sub>3</sub>O<sub>4</sub>-SiO<sub>2</sub> support are nanoflower-spheres with an average diameter of 3.5 μm, self-assembled by numerous Co<sub>3</sub>O<sub>4</sub>-SiO<sub>2</sub> nanosheets (Figure 1A-E). Such structure is endowed with an extremely large surface area of 294 m<sup>2</sup>·g<sup>-1</sup>. The HRTEM image in Figure 1F presents a mixture of crystalline structures with a lattice spacing of 2.86 Å of Co<sub>3</sub>O<sub>4</sub> (220) planes (marked with white box) and amorphous structures of SiO<sub>2</sub> (marked with black circle), further illustrates Co<sub>3</sub>O<sub>4</sub> and SiO<sub>2</sub> embedded by each other. The inset SAED pattern shows polycrystalline diffraction rings, which can be indexed as the (220), (311), (400) and (422) facets of Co<sub>3</sub>O<sub>4</sub>, respectively. In Pt/Co<sub>3</sub>O<sub>4</sub>-SiO<sub>2</sub> nanocomposites, Figure 1G distinctly shows that the Pt NPs (~2 nm) are uniformly dispersed on the surface of Co<sub>3</sub>O<sub>4</sub>-SiO<sub>2</sub>. Its HRTEM image reveals Pt (110) planes with a lattice spacing of 2.27 Å (marked in red box) besides Co<sub>3</sub>O<sub>4</sub> (220) planes and amorphous SiO<sub>2</sub> (Figure 1H). The inset SAED pattern shows mixed diffraction ones of (111) and (220) facets from Pt and (311), (222) and (400) facets from Co<sub>3</sub>O<sub>4</sub>. The further H<sub>2</sub> treatment of the Pt/Co<sub>3</sub>O<sub>4</sub>-SiO<sub>2</sub> lead to the formation of PtCo/Co<sub>3</sub>O<sub>4</sub>-SiO<sub>2</sub> composites, in which the PtCo NPs with a mean diameter of 3 nm are uniformly anchored onto the Co<sub>3</sub>O<sub>4</sub>-SiO<sub>2</sub> nanosheets (Figure 1I). In addition, the mixed crystalline structure proved by the corresponding HRTEM image and SAED patterns confirms the formation of PtCo/Co<sub>3</sub>O<sub>4</sub>-SiO<sub>2</sub> nanocomposite (Figure 1J, K). Figure 1L shows EDS analysis results of the PtCo/Co<sub>3</sub>O<sub>4</sub>-SiO<sub>2</sub> (trace (a)) and Pt/Co<sub>3</sub>O<sub>4</sub>-SiO<sub>2</sub> (trace (b)) composites. Both of them contain Pt, Co, Si and O elements with the atomic ratio of Pt:Co:Si estimated to be 1:20:30, while Pt is absent in the Co<sub>3</sub>O<sub>4</sub>-SiO<sub>2</sub> nanocomposites (trace (c)). The element mappings are shown in Figure 1N-P, which can be overlapped with the corresponding SEM image (Figure 1M).

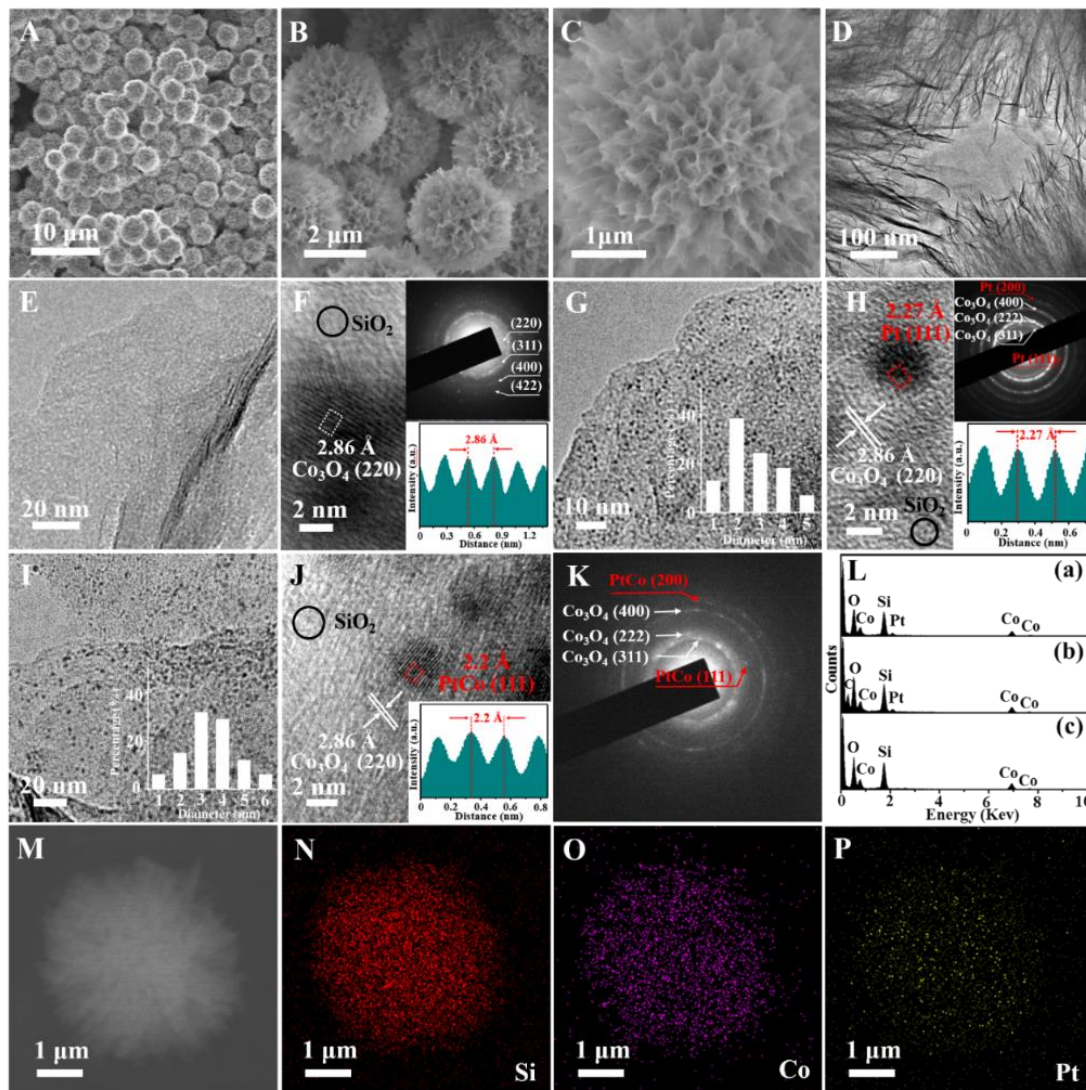


**Figure 1.** (A~C) SEM images and (D, E) TEM images with different magnification of  $\text{Co}_3\text{O}_4\text{-SiO}_2$  nanocomposite; (F) HRTEM image of  $\text{Co}_3\text{O}_4\text{-SiO}_2$  nanocomposite with inset SADE pattern; (G, H) TEM image with inset particle size distribution and HRTEM image with inset SADE pattern of  $\text{Pt/Co}_3\text{O}_4\text{-SiO}_2$  nanocomposite; (I~K) TEM image with inset particle size distribution, HRTEM image and SADE pattern of  $\text{PtCo/Co}_3\text{O}_4\text{-SiO}_2$  nanocomposite; (L) EDS analysis of  $\text{PtCo/Co}_3\text{O}_4\text{-SiO}_2$  (a),  $\text{Pt/Co}_3\text{O}_4\text{-SiO}_2$  (b) and  $\text{Co}_3\text{O}_4\text{-SiO}_2$  (c) nanocomposites; (M~P) SEM image of  $\text{PtCo/Co}_3\text{O}_4\text{-SiO}_2$  nanocomposite and elements mapping of Si, Co and Pt respectively.

Figure 2A shows the XRD patterns of the  $\text{PtCo/Co}_3\text{O}_4\text{-SiO}_2$  nanocomposites and as-contrast samples. Because of the amorphous structure of  $\text{SiO}_2$ , only  $\text{Co}_3\text{O}_4$  peaks can be observed in  $\text{Co}_3\text{O}_4\text{-SiO}_2$  nanocomposite (curve (a)). The similar cases appear in  $\text{Pt/Co}_3\text{O}_4\text{-SiO}_2$  (curve (b)) and

PtCo/Co<sub>3</sub>O<sub>4</sub>-SiO<sub>2</sub> (curve (c)), but without apparent peaks of Pt and PtCo alloys detected. This is mainly because these tiny NPs are uniformly distributed on the surface of Co<sub>3</sub>O<sub>4</sub>-SiO<sub>2</sub>.<sup>12,28</sup> To further confirm the structure of these homodisperse NPs, Pt/Co<sub>3</sub>O<sub>4</sub>-SiO<sub>2</sub> and PtCo/Co<sub>3</sub>O<sub>4</sub>-SiO<sub>2</sub> samples were calcined at 873 K for 5 hrs in an argon environment. The XRD results of these samples were obtained and the results are shown in curves (d) and (e). In curve (d), we can clearly see three peaks at 39.7°, 46.2° and 67.4°, which can be indexed to the (111), (200) and (220) planes of Pt NPs (JCPDF No. 65-6828). Three peaks at 40.3°, 46.8° and 68.0° can be observed in curve (e), which are located between the standard peaks of Pt (JCPDF No. 65-6828) and Co (JCPDF No. 15-0806), indicating the existence of the PtCo NAs.<sup>29,30</sup>

To investigate the redox property of catalyst surface, H<sub>2</sub>-TPR test has been conducted for the PtCo/Co<sub>3</sub>O<sub>4</sub>-SiO<sub>2</sub> nanocomposite and its contrast samples and shown in Figure 2B. There are two reduction peaks in both of the PtCo<sub>sync</sub>/Co<sub>3</sub>O<sub>4</sub>-SiO<sub>2</sub> (curves b) and Pt/Co<sub>3</sub>O<sub>4</sub>-SiO<sub>2</sub> (curves c). The reduction peak in the low temperature range is linked with Co<sup>3+</sup> reduction into Co<sup>2+</sup>, during which the spinel structure of Co<sub>3</sub>O<sub>4</sub> can be converted into CoO. The reduction peak in the high temperature range is related with the reduction of CoO to metallic Co.<sup>31,32</sup> Whereas, the H<sub>2</sub>-TPR curve of the PtCo/Co<sub>3</sub>O<sub>4</sub>-SiO<sub>2</sub> composite (curves a) has three reduction peaks. The weak peak at 166 °C is attributed to the reduction of active lattice oxygen, which derived from SMSI via the in situ alloying of PtCo on Pt/Co<sub>3</sub>O<sub>4</sub>-SiO<sub>2</sub> nanosheets.<sup>33</sup> The active lattice oxygen can significantly enhance the activity of the CO catalytic reaction, especially at the low temperature.<sup>13</sup> In addition, the reduction peak of Co<sup>3+</sup> reduced to Co<sup>2+</sup> has been shifted to higher temperature, which is mainly due to the existence of SMSI between the PtCo NAs and Co<sub>3</sub>O<sub>4</sub>-SiO<sub>2</sub> support.<sup>34</sup>

To examine the role of the active lattice oxygen and PtCo alloy during reaction, we performed CO DRIFTS of PtCo/Co<sub>3</sub>O<sub>4</sub>-SiO<sub>2</sub> nanocomposite (Figure 2C) and compared the results with

Pt/Co<sub>3</sub>O<sub>4</sub>-SiO<sub>2</sub> nanocomposite (Figure 2D). The samples were placed in CO-filled infrared pool at 100°C, and spectral data were collected at 0min, 2min, 5min and 10min, respectively. A prominent symmetrical band at 2174 cm<sup>-1</sup> and 2115 cm<sup>-1</sup> can be observed in both samples, which are assigned to CO in the gas phase and linearly adsorbed CO on catalyst surface, respectively. In addition, a band at 2349 cm<sup>-1</sup> was only seen on PtCo/Co<sub>3</sub>O<sub>4</sub>-SiO<sub>2</sub> for 2min, corresponding to CO<sub>2</sub>, which can be considered as the reaction product of CO adsorbed on the catalyst surface with active lattice oxygen. After 5min, the band of CO<sub>2</sub> disappeared and the band of CO increased, indicating the product CO<sub>2</sub> can desorb in time without affecting CO reabsorption. Whereas for Pt/Co<sub>3</sub>O<sub>4</sub>-SiO<sub>2</sub>, the band of CO keep increasing over time. Therefore, the active lattice oxygen and PtCo alloy plays an important role in the catalytic reaction of CO oxidation.

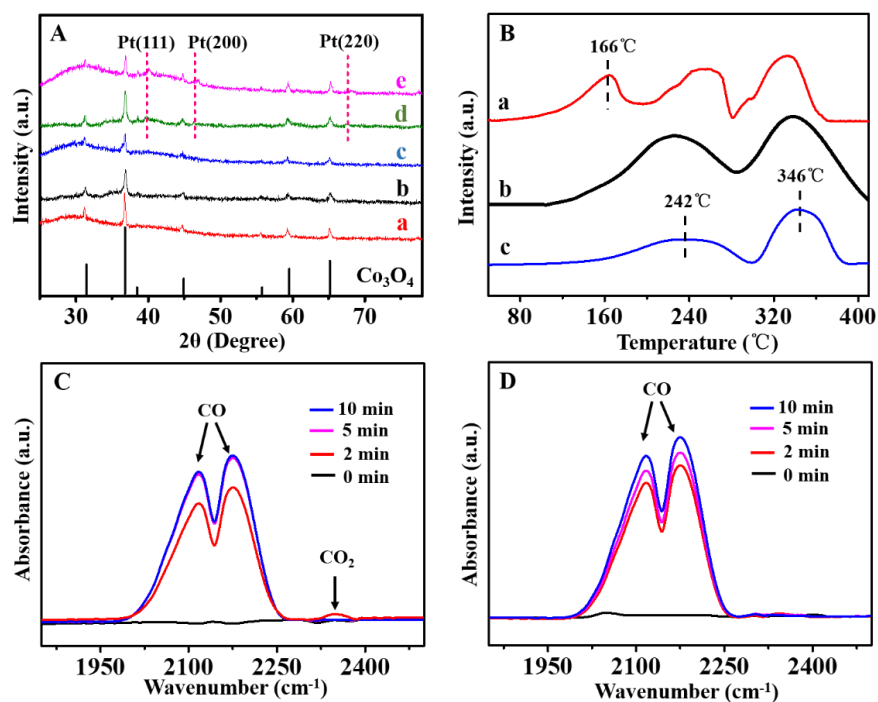


**Figure 2.** (A) XRD patterns of Co<sub>3</sub>O<sub>4</sub>-SiO<sub>2</sub> (a), Pt/Co<sub>3</sub>O<sub>4</sub>-SiO<sub>2</sub> (b), PtCo/Co<sub>3</sub>O<sub>4</sub>-SiO<sub>2</sub> (c), and the annealed Pt/Co<sub>3</sub>O<sub>4</sub>-SiO<sub>2</sub> (d), PtCo/Co<sub>3</sub>O<sub>4</sub>-SiO<sub>2</sub> (e) nanocomposites; (B) H<sub>2</sub>-TPR profiles of PtCo/Co<sub>3</sub>O<sub>4</sub>-SiO<sub>2</sub> (a), PtCo<sub>sync</sub>/Co<sub>3</sub>O<sub>4</sub>-SiO<sub>2</sub> (b) and Pt/Co<sub>3</sub>O<sub>4</sub>-SiO<sub>2</sub> (c) nanocomposites; (C, D) CO DRIFTS of PtCo/Co<sub>3</sub>O<sub>4</sub>-SiO<sub>2</sub> (C) and Pt/Co<sub>3</sub>O<sub>4</sub>-SiO<sub>2</sub> (D).

XPS measurement was performed to further insight into the elemental valence information of Pt/Co<sub>3</sub>O<sub>4</sub>-SiO<sub>2</sub> and PtCo/Co<sub>3</sub>O<sub>4</sub>-SiO<sub>2</sub> nanocomposites. The survey spectra in Figure S4 clearly shows that both of the samples contain C, O, Si, Co, and Pt elements, which are consistent with the EDS results. In order to obtain the specific valence information of the elements, XPSPEAK41 peak software has been used to further analyze the characteristic peaks of Co 2p and Pt 4f. In Figure 3A, the peaks of Pt 4f<sub>7/2</sub> and Pt 4f<sub>5/2</sub> for Pt/Co<sub>3</sub>O<sub>4</sub>-SiO<sub>2</sub> can be deconvoluted into two pairs of peak, the peaks at 71.15 eV and 74.55 eV are attributed to Pt (0), the other peaks at 71.98 eV and 75.48 eV are related to Pt (II). Meanwhile, Pt 4f<sub>7/2</sub> and Pt 4f<sub>5/2</sub> of PtCo/Co<sub>3</sub>O<sub>4</sub>-SiO<sub>2</sub> in Figure 3B can be deconvoluted into two pairs of peak with binding energies of 71.19 eV & 74.7 eV and 72.02 eV & 75.54 eV, corresponding to Pt (0) and Pt (II), respectively. These peaks position of PtCo/Co<sub>3</sub>O<sub>4</sub>-SiO<sub>2</sub> shifts to the higher binding energy compared with those of Pt/Co<sub>3</sub>O<sub>4</sub>-SiO<sub>2</sub>. This is mainly because that after the formation of PtCo alloy, the electron transfer between Pt and Co can shift the binding energy.<sup>35,36</sup> For the detailed XPS analysis of Co 2p spectra, Pt/Co<sub>3</sub>O<sub>4</sub>-SiO<sub>2</sub> (Figure 3C) and PtCo/Co<sub>3</sub>O<sub>4</sub>-SiO<sub>2</sub> (Figure 3D) have the same peak type, both of them are composed of main peaks and satellite peaks, but there is a difference in the position and FWHM of the peaks. Meanwhile, the analysis of XPSPEAK41 peak software shows that the main peaks of Co 2p<sub>3/2</sub> and Co 2p<sub>1/2</sub> for the Pt/Co<sub>3</sub>O<sub>4</sub>-SiO<sub>2</sub> in Figure 3C can be deconvoluted into two pairs of peak with binding energies of 779.8 eV & 795.6 eV and 782.2 eV & 797.2 eV, corresponding to Co (II) and Co (III), respectively. Whereas Figure 3D shows that the peaks of Co 2p<sub>3/2</sub> and Co 2p<sub>1/2</sub> for PtCo/Co<sub>3</sub>O<sub>4</sub>-SiO<sub>2</sub> can be deconvoluted into three pairs of peak with binding energies of 778.7 & 794.6, 780.0 & 795.8 and 782.1 eV & 797.3 eV, corresponding to Co (0), Co (II) and Co (III), respectively. The existence of Co (0) in PtCo/Co<sub>3</sub>O<sub>4</sub>-SiO<sub>2</sub> further demonstrates the successful

partial reduction of Co in Pt/Co<sub>3</sub>O<sub>4</sub>-SiO<sub>2</sub> nanocomposites. The peak located at the binding energy of 103.4 eV is related to the SiO<sub>2</sub> (Figure S5).

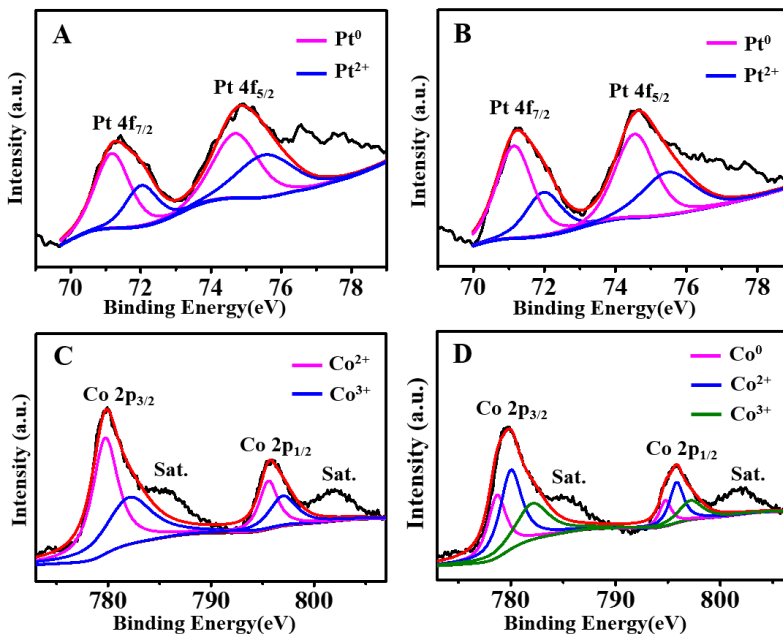


**Figure 3.** Detailed XPS analysis of Pt 4f spectra for Pt/Co<sub>3</sub>O<sub>4</sub>-SiO<sub>2</sub> (A) and PtCo/Co<sub>3</sub>O<sub>4</sub>-SiO<sub>2</sub> (B) as well as Co 2p spectra for Pt/Co<sub>3</sub>O<sub>4</sub>-SiO<sub>2</sub> (C) and PtCo/Co<sub>3</sub>O<sub>4</sub>-SiO<sub>2</sub> (D).

### 3.3. Catalytic Performance

Co<sub>3</sub>O<sub>4</sub> has been widely used as the catalyst for efficient CO oxidation, however its performance stability is still limited by structure stability at high temperature and water vapour at low temperature.<sup>37-39</sup> In order to achieve high structure stability and large surface area for outstanding performance at high temperature, SiO<sub>2</sub> was embedded into Co<sub>3</sub>O<sub>4</sub> to construct Co<sub>3</sub>O<sub>4</sub>-SiO<sub>2</sub> nanosheets. Meanwhile, as relevant density functional theory (DFT) calculation showed that water vapour can effectively promote CO oxidation performance of the Pt based catalyst,<sup>40</sup> Pt was introduced into catalyst system to overcome the negative effects of water vapour. In our case, the as-synthesized heterostructure of PtCo/Co<sub>3</sub>O<sub>4</sub>-SiO<sub>2</sub> is expected to address the issues of Co<sub>3</sub>O<sub>4</sub> structure stability at high temperature and inactivation under water vapour, meanwhile, raising the

catalytic activity of Pt based catalyst at low temperature in virtue of active lattice oxygens derived from the insitu alloying of PtCo from Pt/Co<sub>3</sub>O<sub>4</sub>-SiO<sub>2</sub> under H<sub>2</sub>.

In Figure 4A, for PtCo/Co<sub>3</sub>O<sub>4</sub>-SiO<sub>2</sub> nanocomposites, the CO light-off temperature (T<sub>50</sub>) and the complete conversion temperature (T<sub>100</sub>) are 50 °C and 115 °C, respectively, which are much lower than those of PtCo<sub>sync</sub>/Co<sub>3</sub>O<sub>4</sub>-SiO<sub>2</sub> (T<sub>50</sub> =105 °C and T<sub>100</sub> =155 °C) and Pt/Co<sub>3</sub>O<sub>4</sub>-SiO<sub>2</sub> (T<sub>50</sub> =115 °C and T<sub>100</sub> =170 °C) . The reason can be suggested that the existence of abundant active lattice oxygens in the PtCo/Co<sub>3</sub>O<sub>4</sub>-SiO<sub>2</sub> nanocomposites can remarkably promote the catalytic reaction of CO oxidation. Therefore, the active lattice oxygen plays an important role in the catalytic reaction of CO oxidation. Meanwhile, the activity curve of Co<sub>3</sub>O<sub>4</sub>-SiO<sub>2</sub> nanocomposites shows a U shape, a lowest point of the CO conversion rate at 80 °C can be found, which is mainly due to the influence of water vapour.<sup>41</sup> In addition, the catalytic activity of CO oxidation for PtCo/Co<sub>3</sub>O<sub>4</sub>-SiO<sub>2</sub> nanocomposites have also been compared with other reported catalysts in the literature and summarized in the Table S1. Figure 4B shows the Arrhenius plots of the PtCo/Co<sub>3</sub>O<sub>4</sub>-SiO<sub>2</sub>, PtCo<sub>sync</sub>/Co<sub>3</sub>O<sub>4</sub>-SiO<sub>2</sub>, Pt/Co<sub>3</sub>O<sub>4</sub>-SiO<sub>2</sub> and Co<sub>3</sub>O<sub>4</sub>-SiO<sub>2</sub> composites, according to the slope of the curves, their activation energies can be calculated to be 27.0 kJ/mol, 42.5 kJ/mol, 37.0 kJ/mol and 34.0 kJ/mol, respectively, further demonstrate the best catalytic activity of PtCo/Co<sub>3</sub>O<sub>4</sub>-SiO<sub>2</sub> nanocomposites. Since the light-off curves in Figure 4A can only indicates the short-term performance of the catalyst at a given temperature. In order to further investigate the catalytic activities of the synthesized catalysts in the low temperature and high temperature ranges, we have also tested the catalysts at a constant temperature (50 °C and 400 °C).

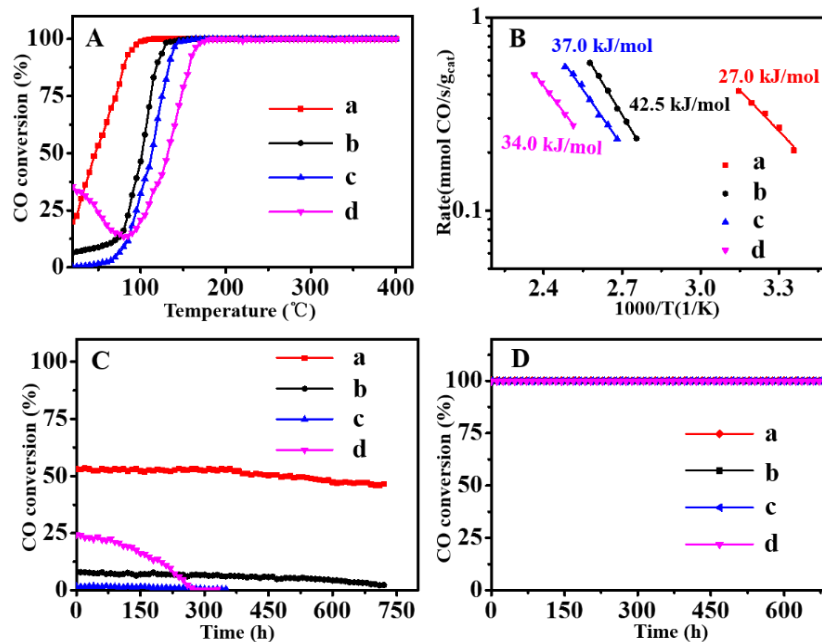


**Figure 4.** Temperature dependence of the activity (A) and Arrhenius plot for CO oxidation (B); Catalytic performance of CO oxidation at a constant temperature of 50 °C (C) and 400 °C (D) for PtCo/Co<sub>3</sub>O<sub>4</sub>-SiO<sub>2</sub> (a), PtCo<sub>sync</sub>/Co<sub>3</sub>O<sub>4</sub>-SiO<sub>2</sub> (b), Pt/Co<sub>3</sub>O<sub>4</sub>-SiO<sub>2</sub> (c) and Co<sub>3</sub>O<sub>4</sub>-SiO<sub>2</sub> (d).

Figure 4C shows the CO conversion rate of PtCo/Co<sub>3</sub>O<sub>4</sub>-SiO<sub>2</sub> nanocomposites and other contrast catalysts, which have been continuously catalysed at 50 °C for 30 days. It can be clearly seen that the Pt/Co<sub>3</sub>O<sub>4</sub>-SiO<sub>2</sub> nanocomposites have little catalytic activity, and the activity of PtCo<sub>sync</sub>/Co<sub>3</sub>O<sub>4</sub>-SiO<sub>2</sub> is much lower than that of the PtCo/Co<sub>3</sub>O<sub>4</sub>-SiO<sub>2</sub>, indicating the formation of PtCo NAs and the active surface lattice oxygens can effectively enhance the catalytic oxidation activity in a low temperature environment. In addition, we can clearly see that catalytic activity of PtCo/Co<sub>3</sub>O<sub>4</sub>-SiO<sub>2</sub> nanocomposites has no significant decrease after 30 days catalysis reaction, by contrast, the catalytic activity of Co<sub>3</sub>O<sub>4</sub>-SiO<sub>2</sub> nanocomposites is decreased sharply after 100 hrs, which mainly because the catalyst surface was deactivated by the water vapour adsorption. Meanwhile, under the high temperature reaction environment of 400 °C, the CO conversion rates for all the synthesized catalysts are 100%, even after 30 days (Figure 4D). It illustrates that the

Co<sub>3</sub>O<sub>4</sub>-SiO<sub>2</sub> support plays a vital role in the catalysis under a high temperature environment. The excellent thermal stability of as-prepared Co<sub>3</sub>O<sub>4</sub>-SiO<sub>2</sub> nanocomposite can be demonstrated by heat treatment at 800 °C in air for 10 hrs (Figure S6).

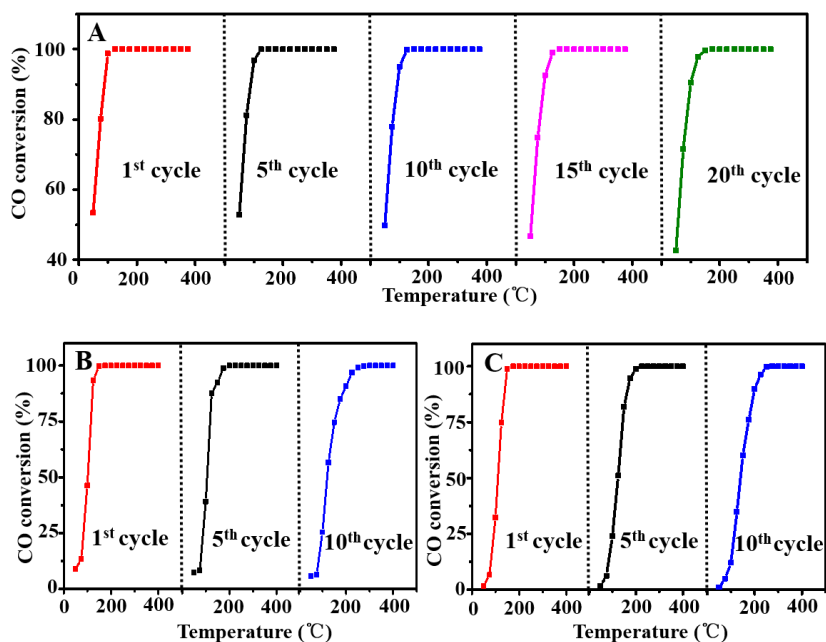
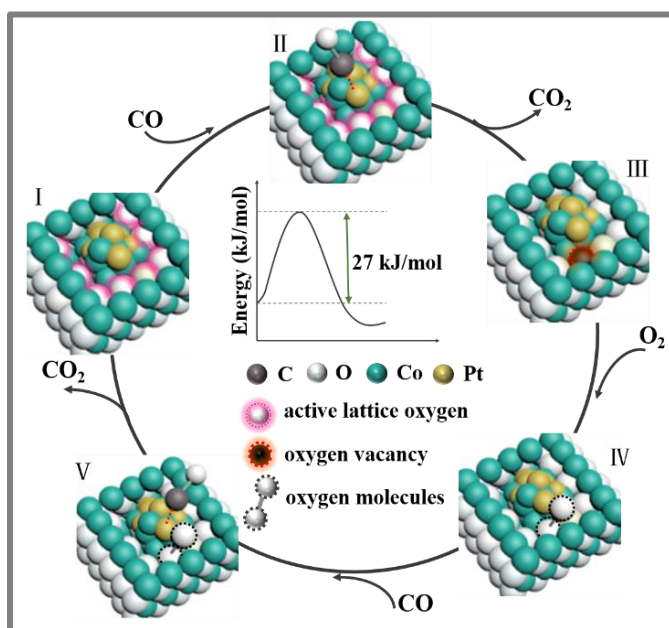


**Figure 5.** Conversion rate of CO from 50 to 400 °C with 20 cycles and 10 cycles for PtCo/Co<sub>3</sub>O<sub>4</sub>-SiO<sub>2</sub> (A), PtCo<sub>sync</sub>/Co<sub>3</sub>O<sub>4</sub>-SiO<sub>2</sub> (B) and Pt/Co<sub>3</sub>O<sub>4</sub>-SiO<sub>2</sub> (C)

For further understand the high temperature thermal cycle stability of the synthesized catalysts, we conducted the cyclic catalytic tests from 50 °C to 400 °C. Figure 5A shows the CO conversion rates of PtCo/Co<sub>3</sub>O<sub>4</sub>-SiO<sub>2</sub> composite cycled for 20 times. The complete conversion temperature T<sub>100</sub> has little increase after 20 cycles. Whereas for the PtCo<sub>sync</sub>/Co<sub>3</sub>O<sub>4</sub>-SiO<sub>2</sub> (Figure 5B) and Pt/Co<sub>3</sub>O<sub>4</sub>-SiO<sub>2</sub> (Figure 5C) nanocomposites after 10 cycles catalysis, the T<sub>100</sub> values are increased from 155 °C to 300 °C and 170 °C to 275 °C, respectively. The morphology and structure of the reacted catalyst have been further investigated by TEM (Figure S7) and XRD characterization (Figure S8). Severe agglomeration can be observed for the PtCo<sub>sync</sub>/Co<sub>3</sub>O<sub>4</sub>-SiO<sub>2</sub> and Pt/Co<sub>3</sub>O<sub>4</sub>-SiO<sub>2</sub> nanocomposites, whereas the PtCo/Co<sub>3</sub>O<sub>4</sub>-SiO<sub>2</sub> only has little increase of the particle size

and there is no obvious change in the phase except adding a broad peak of PtCo alloy, which is mainly due to the increase in the particle size. This demonstrates that the heterostructure of the PtCo/Co<sub>3</sub>O<sub>4</sub>-SiO<sub>2</sub> has better structural stability relative to other nanocomposites, and thus has better cycling stability, which is mainly due to the existence of SMSI between the embedded PtCo NAs and Co<sub>3</sub>O<sub>4</sub>-SiO<sub>2</sub> support.

**Scheme 2. Illustration of the catalysis mechanism of the CO oxidation reaction over PtCo/Co<sub>3</sub>O<sub>4</sub>-SiO<sub>2</sub> nanocomposites.**



Based on the results of structural characterizations and performance measurements, the catalysis mechanism of the PtCo/Co<sub>3</sub>O<sub>4</sub>-SiO<sub>2</sub> nanocomposite has been proposed, as illustrated in Scheme 2. The CO catalytic oxidation can be assumed as a typical gas-solid heterogeneous catalytic reaction, thus the surface microelectronic structures and the specific surface areas of the catalyst have significant influences on its performance. CO oxidation over metallic Pt supported on reducible oxides follows a Mars-van Krevelen reaction mechanism. According to this mechanism, the active lattice oxygens, generated by the insitu alloying of PtCo on Co<sub>3</sub>O<sub>4</sub>-SiO<sub>2</sub> under H<sub>2</sub> reduction treatment, is responsible for the catalytic reaction. Therefore, over the catalyst of

PtCo/Co<sub>3</sub>O<sub>4</sub>-SiO<sub>2</sub> composites, CO is preferentially adsorbed onto the PtCo alloy and then reacts with the active lattice oxygen in its vicinity.<sup>33,42,43</sup> Then the O<sub>2</sub> molecules will fill the oxygen vacancies caused by the reacted lattice oxygen, thus the adsorbed O<sub>2</sub> molecules can be activated and dissociated to easily react with the CO. In addition, the PtCo NAs can weaken the strong absorption of the product CO<sub>2</sub> with Pt which would prevent the re-adsorption of CO at the active sites, thus PtCo/Co<sub>3</sub>O<sub>4</sub>-SiO<sub>2</sub> nanocatalyst have higher catalytic activity and cycle stability than Pt/Co<sub>3</sub>O<sub>4</sub>-SiO<sub>2</sub> nanocatalyst. When the reaction occurs at a high temperature, the influence of the active surface lattice oxygen on the catalytic performance can be significantly decreased, because the high temperature environment is favorable for the breaking of chemical bonds. Therefore, there are no apparent differences in the catalytic activities of CO oxidation among PtCo/Co<sub>3</sub>O<sub>4</sub>-SiO<sub>2</sub>, PtCo<sub>sync</sub>/Co<sub>3</sub>O<sub>4</sub>-SiO<sub>2</sub>, and Pt/Co<sub>3</sub>O<sub>4</sub>-SiO<sub>2</sub> at high temperatures.

#### **4. Conclusion**

In summary, we have designed a flower-like structure of PtCo/Co<sub>3</sub>O<sub>4</sub>-SiO<sub>2</sub> composite, which has been obtained through a galvanic replacement coprecipitation process with subsequent H<sub>2</sub> reduction. The large specific surface areas and excellent structure stability of Co<sub>3</sub>O<sub>4</sub>-SiO<sub>2</sub> significantly enhance the catalytic activity and thermal cycling stability for catalyzing CO oxidation, meanwhile, the abundant active lattice oxygens and the SMSI between PtCo NAs and Co<sub>3</sub>O<sub>4</sub>-SiO<sub>2</sub> support remarkably improve the inferior activity of Pt based catalyst at low temperature. Hence, the PtCo/Co<sub>3</sub>O<sub>4</sub>-SiO<sub>2</sub> nanocomposites present an outstanding enhanced catalytic activity at low temperature and long-term catalytic cyclability for CO oxidation. This work opens up a new way to design a thermostable nanostructures by embedding SiO<sub>2</sub> nanosheets and improve the catalytic activity of catalysts by introducing active centers.

## **ASSOCIATED CONTENT**

### **Supporting Information**

SEM and TEM images, XRD and XPS patterns. This material is available free of charge via the Internet at <http://pubs.acs.org>.

## **AUTHOR INFORMATION**

### **Corresponding Author**

\* E-mail: [m\\_wen@tongji.edu.cn](mailto:m_wen@tongji.edu.cn); Fax: (+86) -21-65981097

### **ORCID**

Ming Wen: 0000-0002-2327-5459

Qingsheng Wu: 0000-0002-2371-5805

### **Author Contributions**

†These authors contributed equally to this work.

### **Notes**

The authors declare no competing financial interest.

## **ACKNOWLEDGMENT**

This work was financially supported by the National Natural Science Foundation of China (NSFC Nos: 21771140, 51271132 and 91222103). UK Engineering and Physical Sciences Research (EPSRC, EP/P018998), Newton Mobility Grant (IE161019) through Royal Society UK and NSFC.

## **ABBREVIATIONS**

NPs, nanoparticles; 2D, two-dimensional; SMSI, strong metal-support interactions; XRD, Powder X-ray diffraction; SEM, scanning electron microscopy; TEM, transmission electron microscopy; HRTEM, high resolution TEM; SAED, selected area electron diffraction; EDS, energy dispersive X-ray spectroscopy; XPS, X-ray photoelectron spectroscopy; BET, Brunauer–Emmett–Teller; H<sub>2</sub>-TPR, H<sub>2</sub> temperature-programmed reduction; CO DRIFTS, CO adsorption diffuse reflectance infrared Fourier-transform spectroscopy; T<sub>50</sub>, light-off temperature; T<sub>100</sub>, complete conversion temperature; NAs, nanoalloys.

## REFERENCES

- [1] Li, Z.; Li, M.; Bian, Z.; Kathiraser, Y.; Kawi, S. Design of Highly Stable and Selective Core/Yolk-Shell Nanocatalysts-A Review. *Appl. Catal. B* **2016**, *188*, 324-341.
- [2] Xiong, H.; Lin, S.; Goetze, J.; Pletcher, P.; Guo, H.; Kovarik, L.; Artyushkova, K.; Weckhuysen, B.M.; Datye, A.K. Thermally Stable and Regenerable Pt-Sn Clusters for Propane Dehydrogenation Prepared via Atom Trapping on Ceria. *Angew. Chem. Int. Ed.* **2017**, *56*, 8986-8991.
- [3] Souza, M. M. V. M.; Schmal, M. Methane Conversion to Synthesis Gas by Partial Oxidation and CO<sub>2</sub> Reforming over Supported Platinum Catalysts. *Catal. Lett.* **2003**, *91*, 11-17.
- [4] Guo, Z.; Liu, B.; Zhang, Q. H.; Deng, W. P.; Wang, Y.; Yang, Y. H.; Recent Advances in Heterogeneous Selective Oxidation Catalysis for Sustainable Chemistry, *Chem. Soc. Rev.* **2014**, *43*, 3480-3524.
- [5] Arai, H.; Machida, M. Thermal Stabilization of Catalyst Supports and Their Application to High-temperature Catalytic Combustion. *Appl. Catal. A* **1996**, *138*, 161-176.
- [6] Chen, A.; Holt-Hindle, P.; Platinum-Based Nanostructured Materials: Synthesis, Properties, and Applications. *Chem. Rev.* **2010**, *110*, 3767-3804.
- [7] Allian, A. D.; Takanabe, K.; Fujdala, K. L.; Hao, X.; Iglesia, E. Chemisorption of CO and Mechanism of CO Oxidation on Supported Platinum Nanoclusters. *J. Am. Chem. Soc.* **2011**, *133*, 4498-4517.

- [8] Chen, W. L.; Ma, Y. L.; Li, F.; Pan, L.; Gao, W. P.; Xiang, Q.; Shang, W.; Song, C. Y.; Tao, P.; Zhu, H.; Pan, X. Q.; Deng, T.; Wu, J. B. Strong Electronic Interaction of Amorphous Fe<sub>2</sub>O<sub>3</sub> Nanosheets with Single-Atom Pt toward Enhanced Carbon Monoxide Oxidation. *Adv. Funct. Mater.* **2019**, 1904278.
- [9] Bonanni, S.; Ait-Mansour, K.; Harbich, W.; Brune, H. Effect of The TiO<sub>2</sub> Reduction State on The Catalytic CO Oxidation on Deposited Size-selected Pt Clusters. *J. Am. Chem. Soc.* **2012**, *134*, 3445-3450.
- [10] Wu, K.; Zhou, L.; Jia, C. J.; Sun, L.; Yan, C. H. Pt-embedded-CeO<sub>2</sub> Hollow Spheres for Enhancing CO Oxidation Performance. *Mater. Chem. Front.* **2017**, *1*, 1754-1763.
- [11] Zhou, H. P.; Wu, H. S.; Shen, J.; Yin, A. X.; Sun, L. D.; Yan, C. H. Thermally Stable Pt/CeO<sub>2</sub> Hetero-nanocomposites With High Catalytic Activity. *J. Am. Chem. Soc.* **2010**, *132*, 4998-4999.
- [12] Jones, J.; Xiong, H.; Delariva, A. T.; Peterson, E. J.; Pham, H.; Challa, S. R.; Qi, G.; Oh, S.; Wiebenga, M. H.; Hernández, X. I. P.; Wang, Y.; Datye, A. K. Thermally Stable Single-atom Platinum-on-ceria Catalysts via Atom Trapping. *Science* **2016**, *353*, 150–154.
- [13] Qiao, B.T.; Wang, A. Q.; Yang, X.F.; Allard, L. F.; Jiang, Z.; Cui, Y. T.; Liu, J. Y.; Li, J.; Zhang, T. Single-atom Catalysis of CO Oxidation Using Pt/FeO<sub>x</sub>. *Nat. Chem.* **2011**, *3*, 634–641.
- [14] Zhang, Z. L.; Zhu, Y. H.; Asakura, H.; Zhang, B.; Zhang, J. G.; Zhou, M. X.; Han, Y.; Tanaka, T.; Wang, A. Q.; Zhang, T.; Yan, N. Thermally Stable Single Atom Pt/m-Al<sub>2</sub>O<sub>3</sub> for Selective Hydrogenation and CO Oxidation. *Nat. Commun.* **2017**, *8*, ncomms16100.
- [15] Tan, C. L.; Cao, X. H.; Wu, X. J.; He, Q. Y.; Yang, J.; Zhang, X.; Chen, J. Z.; Zhao, W.; Han, S. K.; Nam, G. H.; Sindoro, M.; Zhang, H. Recent Advances in Ultrathin Two-dimensional Nanomaterials. *Chem. Rev.* **2017**, *117*(9), 6225-6331.
- [16] Zhang, H. Ultrathin Two-dimensional Nanomaterials. *ACS nano* **2015**, *9*, 9451-9469.
- [17] Zhang, X.; Xie, Y. Recent Advances in Free-standing Two-dimensional Crystals with Atomic Thickness: Design, Assembly and Transfer Strategies. *Chem. Soc. Rev.* **2013**, *42*, 8187-8199.
- [18] Sun, Y.; Gao, S.; Xie, Y. Atomically-thick Two-dimensional Crystals: Electronic Structure Regulation and Energy Device Construction. *Chem. Soc. Rev.* **2014**, *43*, 530-546.
- [19] Wu, D. D.; Wen, M.; Lin, X. J.; Wu, Q. S.; Gu, C.; Chen, H. X. A NiCo/NiO-CoO<sub>x</sub> Ultrathin Layered Catalyst with Strong Basic Sites for High-performance H<sub>2</sub> Generation from Hydrous Hydrazine. *J. Mater. Chem. A* **2016**, *4*, 6595-6602.

- [20] Wu, D. D.; Wen, M.; Gu, C.; Wu, Q. S. 2D NiFe/CeO<sub>2</sub> Basic-site-enhanced Catalyst via In-situ Topotactic Reduction for Selectively Catalyzing the H<sub>2</sub> Generation from N<sub>2</sub>H<sub>4</sub>·H<sub>2</sub>O. *ACS Appl. Mater. Interfaces* **2017**, *9*, 16103-16108.
- [21] Gu, C.; Wu, D. D.; Wen, M.; Wu, Q. S. A Freestanding SiO<sub>2</sub> Ultrathin Membrane with NiCu Nanoparticles Embedded on Its Double Surfaces for Catalyzing Nitro-amination. *Dalton Trans.* **2018**, *47*, 7083-7089.
- [22] Sun, Y.; Liu, Q.; Gao, S.; Cheng, H.; Xie, Y. Pits Confined in Ultrathin Cerium (IV) Oxide for Studying Catalytic Centers in Carbon Monoxide Oxidation. *Nat. Commun.* **2013**, *4*, 2899.
- [23] Hu, Y.; Tao, K.; Wu, C.; Zhou, C.; Yin, H.; Zhou, S. Size-controlled Synthesis of Highly Stable and Active Pd@SiO<sub>2</sub> Core-shell Nanocatalysts for Hydrogenation of Nitrobenzene. *J. Phys. Chem. C* **2013**, *138*, 8974–8982.
- [24] Masoud, N.; Delannoy, L.; Schaik, H.; Eerden, A. V. D.; Rijk, J. W. D.; Silva, T. A. G.; Banerjee, D.; Meeldijk, J. D.; Jong, K. P. D.; Louis, C.; Jongh, P. E. D. Superior Stability of Au/SiO<sub>2</sub> Compared to Au/TiO<sub>2</sub> Catalysts for the Selective Hydrogenation of Butadiene. *ACS Catal.* **2017**, *7*, 5594-5603.
- [25] Zhu, S.; Lian, X.; Fan, T.; Chen, Z.; Dong, Y.; Weng, W.; Yi, X.; Fang, W. Thermally Stable Core-shell Ni/nanorod-CeO<sub>2</sub>@SiO<sub>2</sub> Catalyst for Partial Oxidation of Methane at High Temperatures. *Nanoscale* **2018**, *10*, 14031-14038.
- [26] Fang, H.; Yang, J. H.; Wen, M.; Wu, Q. S. Nanoalloy Materials for Chemical Catalysis. *Adv. Mater.* **2018**, 1705698.
- [27] Wang, D.; Li, Y. One-pot Protocol for Au-based Hybrid Magnetic Nanostructures via a Noble-metal-induced Reduction Process. *J. Am. Chem. Soc.* **2010**, *132*, 6280-6281.
- [28] Zhang, R. B.; Lu, K.; Zong, L. J.; Tong, S.; Wang, X. W.; Feng, G. Gold Supported on Ceria Nanotubes for CO Oxidation. *Appl. Surf. Sci.* **2017**, *416*, 183-190.
- [29] Wang, H. L.; Yan, J. M.; Wang, Z. L.; O, S.; Jiang, Q. Highly Efficient Hydrogen Generation from Hydrous Hydrazine over Amorphous Ni<sub>0.9</sub>Pt<sub>0.1</sub>/Ce<sub>2</sub>O<sub>3</sub> Nanocatalyst at Room Temperature. *J. Mater. Chem. A* **2013**, *1*, 14957-14962.
- [30] Wu, D. D.; Zhang, Y. Q.; Wen, M.; Fang, H.; Wu, Q. S. Fe<sub>3</sub>O<sub>4</sub>/FeNi Embedded Nanostructure and Its Kinetic Law for Selective Catalytic Reduction of *p*-nitrophenyl Compounds. *Inorg. Chem.* **2017**, *56*, 5152-5157.

- [31] Tang, C. W.; Kuo, M. C.; Lin, C. J.; Wang, C. B.; Chien, S. H. Evaluation of Carbon Monoxide Oxidation Over CeO<sub>2</sub>/Co<sub>3</sub>O<sub>4</sub> Catalysts: Effect of Ceria Loading. *Catal. Today* **2008**, *131*, 520-525.
- [32] Min, K.; Min, W. S.; Chang, H. L. Catalytic Carbon Monoxide Oxidation over CoO<sub>x</sub>/CeO<sub>2</sub> Composite Catalysts. *Appl. Catal. A* **2003**, *251*, 143-156.
- [33] Nie, L.; Mei, D.; Xiong, H.; Peng, B.; Ren, Z.; Hernandez, X.I.P.; DeLaRiva, A.; Wang, M.; Engelhard, M.H.; Kovarik, L.; Datye, A.K.; Wang, Y. Activation of Surface Lattice Oxygen in Single-atom Pt/CeO<sub>2</sub> for Low-temperature CO Oxidation. *Science* **2017**, *358*, 1419-1423.
- [34] Tang, C. W.; Kuo, C. C.; Kuo, M. C.; Wang, C. B.; Chien, S. H. Influence of Pretreatment Conditions on Low-temperature Carbon Monoxide Oxidation over CeO<sub>2</sub>/Co<sub>3</sub>O<sub>4</sub> Catalysts. *Appl. Catal. A* **2006**, *309*, 37-43.
- [35] Fang, H.; Chen, Y.; Wen, M.; Wu, Q. S.; Zhu, Q. J. SnNi Nanoneedles Assembled 3D Radial Nanostructure Loaded with SnNiPt Nanoparticles : Towards Enhanced Electrocatalysis Performance for Methanol Oxidation. *Nano Res.* **2017**, *10*, 3929-.
- [36] Wang, W.; Wang, Z. Y.; Wang, J. J.; Zhong, C. J.; Liu, C. J. Highly Active and Stable Pt-Pd Alloy Catalysts Synthesized by Room-Temperature Electron Reduction for Oxygen Reduction Reaction. *Adv. Sci.* **2017**, *4*, 1600486.
- [37] Xie, X.; Li, Y.; Liu, Z. Q.; Haruta, M.; Shen, W. Low-Temperature Oxidation of CO Catalysed By Co<sub>3</sub>O<sub>4</sub> Nanorods. *Nature* **2009**, *458*, 746-749.
- [38] Tüysüz, H.; Comotti M.; Schüth, F. Ordered Mesoporous Co<sub>3</sub>O<sub>4</sub> as Highly Active Catalyst for Low Temperature CO-oxidation. *Chem. Commun.* **2008**, *34*, 4022-4024.
- [39] Liotta, L. F.; Wu, H.; Pantaleo, G.; Venezia, A. M. Co<sub>3</sub>O<sub>4</sub> Nanocrystals and Co<sub>3</sub>O<sub>4</sub>-MO<sub>x</sub> Binary Oxides for CO, CH<sub>4</sub> and VOC Oxidation at Low Temperatures: A Review. *Catal. Sci. Technol.* **2013**, *3*, 3085-3102.
- [40] Wang, H.; Richard, K.; Guo, Y.; Lu, G.Z.; Hu, P. Structural Origin: Water Deactivates Metal Oxides to CO Oxidation And Promotes Low-temperature CO Oxidation With Metals. *Angew. Chem., Int. Ed.* **2012**, *51*(27), 6657-6661.
- [41] Jia, C. J.; Schwickardi, M.; Weidenthaler, C.; Schmidt, W.; Korhonen, S.; Weckhuysen, B. M.; Schüth, F. Co<sub>3</sub>O<sub>4</sub>-SiO<sub>2</sub> Nanocomposite: A Very Active Catalyst for CO Oxidation with Unusual Catalytic Behavior. *J. Am. Chem. Soc.* **2011**, *133*, 11279-11288.

- [42] Kopelent, R.; van Bokhoven, J.A.; Szlachetko, J.; Edebeli, J.; Paun, C.; Nachtegaal, M.; Safonova, O.V. Catalytically Active and Spectator Ce<sup>3+</sup> In Ceria-Supported Metal Catalysts. *Angew. Chem., Int. Ed.* **2015**, *54*, 8728-8731.
- [43] Liu, H. H.; Wang, Y.; Jia, A. P.; Wang, S. Y.; Luo, M. F.; Lu, J. Q. Oxygen Vacancy Promoted CO Oxidation over Pt/CeO<sub>2</sub> Catalysts: A Reaction at Pt-CeO<sub>2</sub> Interface. *Applied Surface Science* **2014**, *314*, 725-734.

## Table of Contents

An ultra-stable PtCo/Co<sub>3</sub>O<sub>4</sub>-SiO<sub>2</sub> nanocatalyst with active surface lattice oxygen have been explored to overcome the issues of Co<sub>3</sub>O<sub>4</sub>-SiO<sub>2</sub> inactivation by water vapor and the Pt inferior activity at low temperature for catalyzing CO oxidation.

**Keywords:** PtCo/Co<sub>3</sub>O<sub>4</sub>-SiO<sub>2</sub>, flower-like structure, CO oxidation, active lattice oxygen, long-term durability

### Authors:

Dandan Wu,<sup>†a,b</sup> Runping Jia<sup>†,b</sup>, Ming Wen<sup>\*,a</sup>, Shuai Zhong<sup>a</sup>, Qingsheng Wu<sup>a</sup>, YongQing Fu<sup>c</sup>, Shuhong Yu<sup>d</sup>,

### Title:

Ultra-stable PtCo/Co<sub>3</sub>O<sub>4</sub>-SiO<sub>2</sub> Nanocomposite with Active Lattice Oxygen for Superior Catalytic Activity towards CO Oxidation

